Nano Research
2019, 12(7): 1663–1667

ISSN 1998-0124 CN 11-5974/O4
https://doi.org/10.1007/s12274-019-2417-5

Research Article

# Spectroscopic signatures of edge states in hexagonal boron nitride

Chuang Gao[1,§], Lei Tao[1,2,3,§], Yu-Yang Zhang[1,4] (✉), Shixuan Du[1,2,4], Sokrates T. Pantelides[1,3], Juan Carlos Idrobo[5], Wu Zhou[1,4] (✉), and Hong-Jun Gao[1,2,4]

[1] *School of Physical Sciences and CAS Key Laboratory of Vacuum Physics, University of Chinese Academy of Sciences, Beijing 100049, China*
[2] *Institute of Physics, Chinese Academy of Sciences, Beijing 100190, China*
[3] *Department of Physics and Astronomy and Department of Electrical Engineering and Computer Science, Vanderbilt University, Nashville, TN 37235, USA*
[4] *CAS Centre for Excellence in Topological Quantum Computation, University of Chinese Academy of Sciences, Beijing 100049, China*
[5] *Center for Nanophase Materials Sciences, Oak Ridge National Laboratory, Oak Ridge, TN 37831, USA*
[§] *Chuang Gao and Lei Tao contributed equally to this work.*


**Received:** 6 March 2019 / **Revised:** 3 April 2019 / **Accepted:** 12 April 2019

## ABSTRACT

We use Z-contrast imaging and atomically resolved electron energy-loss spectroscopy on an aberration-corrected scanning transmission electron microscope to investigate the local electronic states of boron atoms at different edge structures in monolayer and bilayer h-BN. We find that edges with bonding unsaturated $sp^2$ boron atoms have a unique spectroscopic signature with a prominent pre-peak at ~ 190.2 eV in the B K-edge fine structure. First-principles calculations reveal that the observed pre-peak arises from excitations to the in-plane lowest-energy empty $sp^2$ boron dangling bonds at the B-terminated edge. This spectroscopic signature can serve as a fingerprint to explore new edge structures in h-BN.

## KEYWORDS

h-BN, edge structure, spectroscopic signatures, electron energy-loss near edge structure

## 1 Introduction

Defects in hexagonal boron nitride (h-BN), a two-dimensional (2D) insulator with honeycomb structure, have attracted much attention, as their atomic structure and local properties may differ from those in graphene due to the presence of two different elements. Many defect configurations have been reported in atomically thin h-BN, including atomic vacancies [1], reconstructed edges [1, 2], and grain boundaries [3, 4]. Novel properties have also been observed, such as room-temperature ultrabright single-photon emission and photoluminescence upconversion, from defects in h-BN [5, 6]. In addition, spin-polarized states have been predicted to be present at the zigzag edges of h-BN nanoribbons and transitions between metallic, semiconducting and half-metallic states can be achieved by applying an external electric field [7]. Further investigation of edge states at the atomic scale can contribute to understanding the interesting local properties that may emerge in these 1D defects in h-BN nanosheets.

Scanning tunneling microscopy (STM) and scanning tunneling spectroscopy (STS) have been used to reveal the defect structures and related electronic properties in h-BN [8–10]. Besides STM/STS, aberration corrected scanning transmission electron microscopy (STEM) has demonstrated powerful capabilities in atomic-resolution imaging and spectroscopy. It has been possible to analyze the local electronic structures atom-by-atom by combining annular dark-field (ADF) imaging with electron energy-loss spectroscopy (EELS) in STEM [11–17]. ADF imaging identifies the positions of the target atoms and distinguishes the elements via atomic number ($Z$) contrast; while simultaneously-acquired energy-loss near-edge structure (ELNES) in EELS can reveal the bonding and local electronic structure of the target atoms. Recently, such approaches have been applied to reveal the bonding configurations of single silicon dopant atoms in graphene [13, 18], the spin states of individual transition-metal atoms in a graphene lattice [19], and the signature of local electronic states from singly-, doubly-, and triply-coordinated C atoms at the graphene edge [11, 20]. In monolayer h-BN, Suenaga et al. have demonstrated that the spectroscopic signature of a boron vacancy can be distinguished as a pre-peak in the N K-edge ELNES due to the presence of dangling bonds at neighboring nitrogen atoms [21]. However, spectroscopic signatures of boron atoms with dangling bonds have not been reported.

In this article, we investigate the spectroscopic signatures of local electronic states from four representative types of edge structures in monolayer and bilayer h-BN, namely i) boron terminated zigzag edge and ii) nitrogen terminated zigzag edge in monolayer h-BN; iii) step edges in bilayer h-BN, and iv) bilayer closed edge. The atomic configurations of the edges are unambiguously identified by STEM-ADF imaging with single-atom sensitivity, while the local electronic states of B atoms at the edges of h-BN are revealed by atomic resolution ELNES combined with first-principles calculations. A prominent pre-peak is observed in the B K-edge ELNES from B terminated zigzag edges in monolayer h-BN and bilayer step edges, while this spectroscopic signature is absent at the N-terminated zigzag edges in monolayer and bilayer h-BN. Density functional theory (DFT) calculations reproduce the main feature of B K-edge ELNES, and the electron distribution indicates that this prominent pre-peak arises from dangling bonds of B atoms along the B-terminated zigzag edges. In bilayer edges where the top and bottom h-BN layers undergo edge reconstruction to form a closed loop [22], no such pre-peak is present due to saturation of B bonding, but a

Address correspondence to Wu Zhou, wuzhou@ucas.ac.cn; Yu-Yang Zhang, zhangyuyang@ucas.ac.cn

drastic change of the intensity ratio between the B K-edge $\pi^*$ and $\sigma^*$ peaks is observed. Our results provide a direct measurement of the local edge states in insulating h-BN at the atomic scale, which could be difficult to obtain by other experimental methods.

## 2 Experimental

The experiments were performed on thin flakes of h-BN grown by chemical vapor deposition [23]. The sample was transferred onto a TEM grid using a poly-(methyl-methacrylate) (PMMA) assisted method [23]. An aberration corrected Nion UltraSTEM operated at 60 kV was used for atomic resolution ADF imaging and EELS analysis. The monolayer and bilayer edges are created *in-situ* by using the electron beam to sputter out B and N atoms and peel off the h-BN flakes layer-by-layer. Edges created this way are typically free of contamination and are in their pristine state without hydrogen passivation, as hydrogen atoms can be easily knocked out by the 60 kV electron beam. EELS analysis was performed in line-scan mode, with step size of ~ 0.02 nm and exposure time of 0.2 s/pixel, in order to minimize irradiation damage to the edge structures during EELS analysis. The probe current was set to about 50 pA and the convergence semi-angle was about 30 mrad. The EELS collection semi-angle was set to ~ 48 mrad, and the ADF images were collected from ~ 75 to 200 mrad.

## 3 Results and discussion

Figures 1(a) and 1(d) show the typical STEM-ADF images of B- and N-terminated zigzag edges in monolayer h-BN, with the overlaid structural models shown in Figs. 1(b) and 1(e). The number of layers for thin h-BN flakes can be identified via quantitative analysis of the STEM-ADF image intensity, as shown in Fig. S1 in the Electronic Supplementary Material (ESM). Owing to the Z-contrast nature of the STEM-ADF imaging, the B and N atoms in the monolayer lattice can be unambiguously identified from the image intensity, with N atoms being brighter than the B atoms. The termination of the edges can then be easily determined from the orientation of the h-BN lattice. It can be noted that apart from the out-most terminating B or N atoms along the zigzag edges, all other atoms have the same local three-fold bonding configuration as in the bulk structure.

In order to explore the possible changes in electronic states at these monolayer zigzag edges due to the presence of unsaturated bonding, STEM-EELS line-scans were acquired across the two edges, from the bulk lattice into vacuum, as illustrated by the arrows in Figs. 1(b) and 1(e). The simultaneously acquired ADF signals were used to locate the positions of the terminating edge atoms. The B K-edge ELNES extracted from the edge and the bulk lattice are shown in Fig. 1(c). The spectrum obtained in the bulk lattice shows typical spectroscopy fine structures of $sp^2$ bonded B atoms with a sharp $\pi^*$ peak at 191.7 eV, followed by a strong $\sigma^*$ peak at 198.6 eV. In contrast, the spectrum extracted from the terminating B atom at the zigzag edge shows a prominent pre-peak at 190.2 eV, associated with a noticeable reduction of the intensity from the typical $\pi^*$ and $\sigma^*$ peaks (see Fig. S2 in the ESM). It should be noted that this new spectroscopic feature is highly localized only at the terminating B atom at the B-zigzag edge, indicating that it is closely related to the unique twofold coordination of the B atoms at the B-terminated zigzag edge.

For comparison, the B K-edge ELNES extracted from the N-terminated zigzag edge closely resembles that from the bulk lattice, and no pre-peak is observed for the B K-edge. This behaviour can be expected, as ELNES is mainly affected by bonding with nearest neighbours, and the B atoms at the N-terminated zigzag edge essentially have the same bonding configuration as those in the bulk lattice. It is noteworthy that, within the signal-to-noise level of our experiment, the N K-edge ELNES at the N-terminated zigzag edge is similar to the N K-edge ELNES in the bulk lattice, without any pre-peak (see Fig. S3 in the ESM). This behaviour is different from

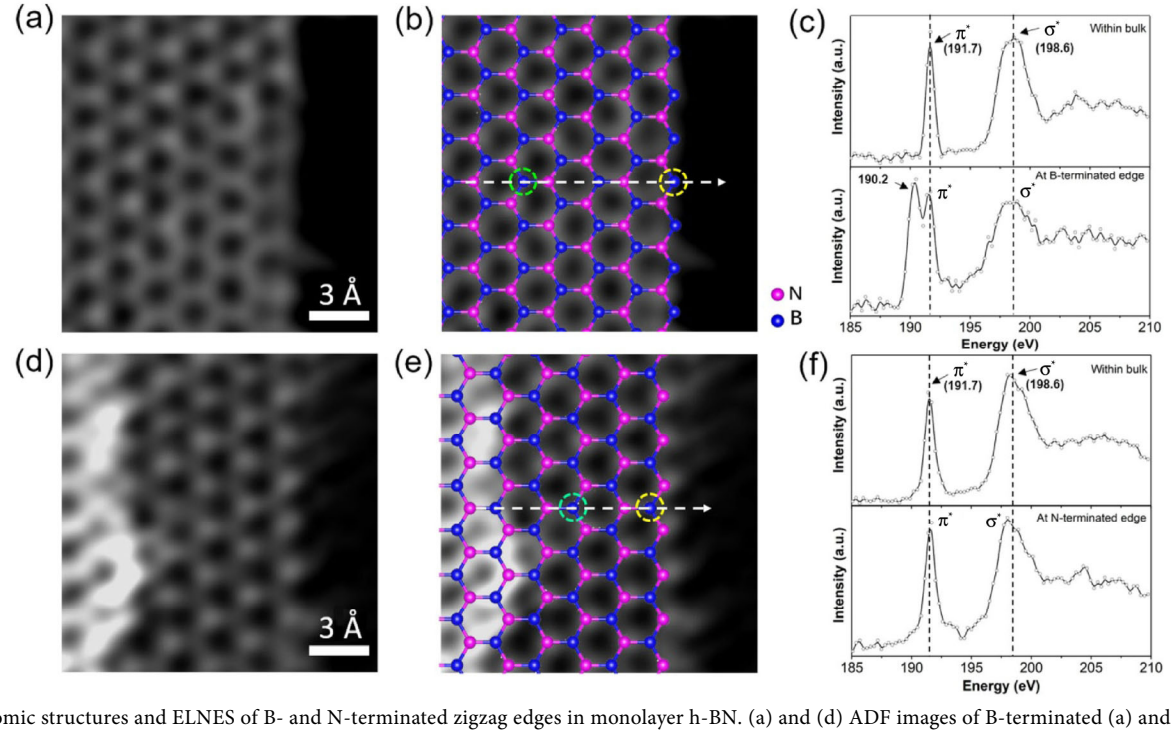


**Figure 1** Atomic structures and ELNES of B- and N-terminated zigzag edges in monolayer h-BN. (a) and (d) ADF images of B-terminated (a) and N-terminated (d) zigzag edges. (b) and (e) The corresponding atomic structural models overlaid on the ADF images. The B and N atoms are shown in blue and purple, respectively. (c) and (f) ELNES of B K-edge extracted from EELS line scans across a B-terminated (c) and a N-terminated (f) zigzag edge. Spectra from B atoms along the edges and within the bulk are compared. The arrows in (b) and (e) illustrate the EELS line scan trajectories across the edges, while the circles illustrate the positions where the spectra in (c) and (f) were extracted. Note that the ADF images and the spectra from EELS line scans were taken from different datasets (see the ESM for the associated ADF images for the EELS line scans).

that of a B vacancy, where a pre-peak in the N K-edge spectrum was identified and attributed to the dangling bonds at neighbouring N atoms [21]. This discrepancy may well be due to the relatively low signal-to-noise (*S*/*N*) for the N K-edge in our experimental data, which is not sufficient to resolve the low intensity pre-peak. Figure S6 in the ESM shows the calculated N K-edge within bulk h-BN and at a N-terminated edge. A pre-peak is present at 397.7 eV, but the intensity is very weak compared to the $\pi^*$ peak at 403.3 eV.

To further verify that the prominent pre-peak in the B K-edge ELNES arises from dangling bonds of edge B atoms, we performed atomically-resolved STEM-EELS line scans from bilayer h-BN edges. It has been reported that the complementary B- and N-terminated zigzag edges in the two AA′-stacked h-BN layers would spontaneously undergo reconstruction and form closed edges with bonding across the two layers [22]. Continuous electron irradiation of a bilayer h-BN film peels off the material layer-by-layer and holes through both layers can be easily created as shown in Fig. 2(a) (see Fig. S1 in the ESM for the identification of number of layers). The equal intensity at the atomic sites within the hexagonal rings indicates that the bilayer BN adopts AA′ stacking, while the orientation of each layer as shown in Fig. 2(b) can be identified from the exposed monolayer region where the top layer h-BN is sputtered (see Fig. S4 in the ESM). Even though the bilayer edges at opposite sides of the hole have different orientations, they are structurally equivalent, with the N-terminated zigzag edge in one layer bonded to the B-terminated zigzag edge in the other. Figures 2(c)–2(e) show the B K-edge fine structures extracted within the bulk and at the left and the right edges of the hole. In sharp contrast to the spectra from monolayer edges, the B K-edge ELNES acquired at the bilayer edges shows no sign of the aforementioned pre-peak of the B K-edge. However, a drastic increase of the intensity of the $\pi^*$ peak with respect to the $\sigma^*$ peak is clearly observed at the bilayer edges, as compared to the bulk spectrum, which is consistent with the reported characters of the B K-edge ELNES of closed edge in bilayer h-BN [22]. The missing of the prominent pre-peak in the B K-edge ELNES is also consistent with the bilayer closed edge model without dangling bond at the B atoms along the edges (Fig. 2(b)).

In order to elucidate the origins of the spectroscopic features in the experimental EELS data, we carried out DFT calculations to simulate the ELNES at monolayer and bilayer edges. The calculations were performed using the Vienna *ab initio* simulation package (VASP) with the projected augmented wave (PAW) method [24, 25]. Wave functions were expanded in a plane-wave basis set to 600-eV energy cutoff. Exchange and correlation effects were described by the Perdew-Burke-Ernzerhof version. A Z+1 model was applied to include the effect of the core hole on the excited electron [26, 27]. Core level EELS was simulated using the partial density of states (pDOS) projected on the p orbitals with a smearing width of 0.5 eV. A nanoribbon model with hydrogen atom passivation at one side, containing 8 unit cells in the periodic direction and 10 unit cells in the perpendicular direction, was used to simulate a monolayer B- or N-terminated edge, while a 10 × 16 supercell was used to simulate the bilayer edges. All structures were fully relaxed until the net force is less than 0.02 eV/Å. The Brillouin zone was sampled with 2 × 1 × 1 points for monolayer B- or N-terminated edges and 1 × 1 × 1 for bilayer edges [28].

In monolayer BN, the simulated ELNES of a boron atom in the bulk material, at a B-terminated zigzag edge, and at a N-terminated edge are shown in black, red and blue, respectively, in Fig. 3(a). The spectra have been shifted by the same amount so that the first peak in the bulk spectrum matches with the peak in the experimental spectrum at 191.7 eV (marked by the green arrow). The main features of the experimental ELNES can all be well reproduced by the theoretical simulations, including a sharp peak at 191.7 eV in all ELNES and a strong pre-peak at 190.0 eV (marked by the purple arrow, experimental value at 190.2 eV) for the boron atom located at a monolayer B-terminated zigzag edge.

The electron density distribution of the excited state at 191.7 eV indicates that the lowest unoccupied state within the bulk comprises the $p_z$ orbital, i.e., it is a $\pi^*$ peak, as shown in Fig. 3(c). Similarly, the excitation at 191.7 eV ($\pi^*$ peak) for the boron atom located at the B-terminated edge also comprises an unoccupied $p_z$ orbital (Fig. 3(e)). In contrast, an $sp^2$-like orbital is the main component of the lowest-energy unoccupied molecular orbital (LUMO) at 190.0 eV (Fig. 3(d)), suggesting the excitation is mainly from 1s orbitals to a boron dangling bonds at the B-terminated edge. No pre-peak shows

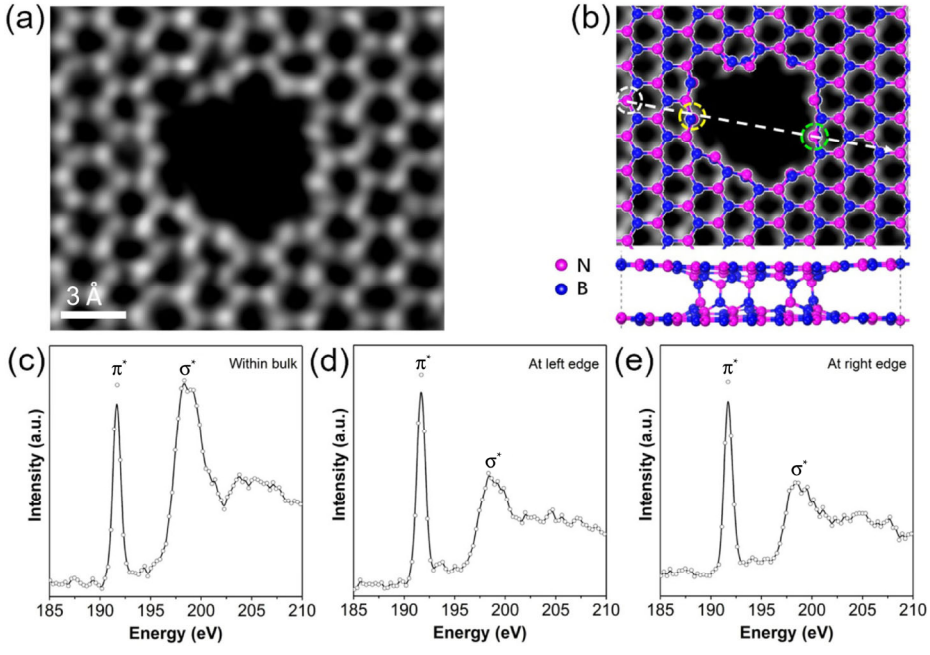


**Figure 2** ADF imaging and ELNES from bilayer h-BN edges. (a) ADF image of a bilayer h-BN region with a nm-sized hole generated by electron beam irradiation. (b) Top and side views of the DFT relaxed structural model overlaid on the ADF image. (c)–(e) ELNES of B K-edge extracted from the EELS line scan across the bilayer edges, as indicated by the white arrow. The corresponding positions where the spectra were extracted are labelled by the white, yellow and green circles, respectively.

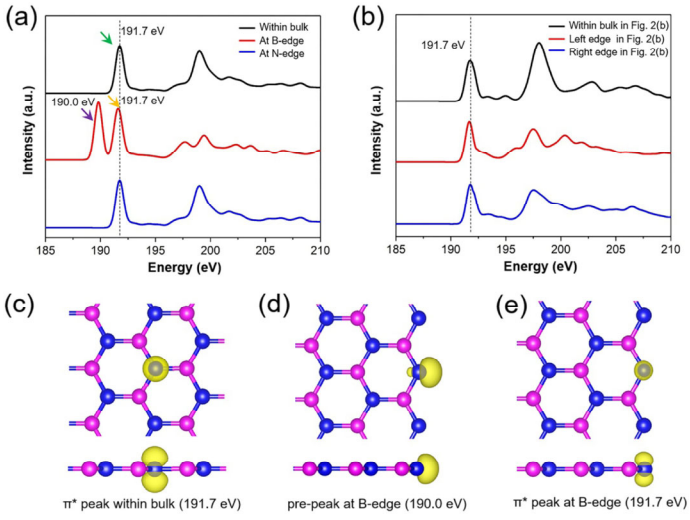


**Figure 3** ELNES simulation of boron K-edge in different structures of h-BN. (a) Simulated ELNES of a boron atom in monolayer B- and N-terminated zigzag edge structures. The black, red and blue lines are the simulated B K-edge spectra within bulk, at a B-terminated edge and at a N-terminated edge, respectively. (b) Simulated ELNES of a boron atom in the reconstructed bilayer region based on the structural model in Fig. 2(b). The black, red and blue lines are the simulated spectra within bulk (white circle marked in Fig. 2(b), at the left edge (yellow circle), and the right edge (green circle), respectively. (c) Electron density of a B atom showing the distribution of excited states at 191.7 eV within bulk (marked by green arrow in (a)). (d) and (e) Electron density of a B atom showing the distribution of excited states at 190.0 and 191.7 eV at a monolayer B-terminated edge, marked by the purple and yellow in (a), respectively. The upper and lower panels are the top views and the side views. The isosurface is 0.015 e/Bohr$^3$.

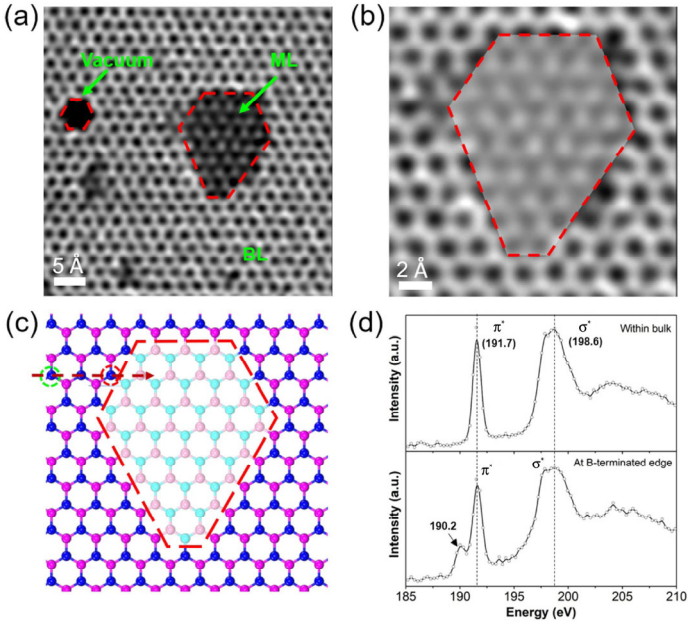


**Figure 4** ADF imaging and ELNES from bilayer h-BN step edges. (a) ADF image of bilayer h-BN with a monolayer region and step edges. (b) A zoom-in ADF image of the h-BN bilayer step edges in (a). The outline of the step edges is highlighted by the red dash line. (c) A schematic structural model of the step edges shown in (b), highlighting the B/N terminated zigzag step-edges. (d) ELNES of B K-edge extracted from EELS line scan across the step edge along the arrow direction as shown in (c). The ELNES from the B atoms along the edge and within bulk are compared.

up at the monolayer N-terminated zigzag edge (Fig. 3(a)) as the B $p_x$ and $p_y$ orbitals are fully occupied at the N-terminated edge. Another noticeable feature is that the intensity of both the $\pi^*$ and the $\sigma^*$ peaks at B-terminated edges is weaker than the corresponding intensity within the bulk, which is consistent with the experimental data in Fig.1(c). The electron density map of unoccupied states for the $\sigma^*$ peak in Fig. S7 in the ESM further confirms that the electron density at B-terminated edges is significantly lower than the corresponding density within the bulk, indicating there is electron rearrangement at the B edge from the $\sigma^*$ peak to the boron dangling bond.

In the bilayer simulations, DFT relaxation yields a model with interlayer B-N bonding at the bilayer edges (Fig. 2(b)). No pre-peak is present at either of the bilayer reconstructed edges as shown in Fig. 3(b), consistent with the absence of dangling bonds. Notably, a reversal of the $\pi^*$ to $\sigma^*$ peak intensity ratio at the reconstructed bilayer edges, as also observed in the experiment, indicates that the orbital intensity is larger comparing to the flat bilayer region because of structural distortions, which is consistent with a previous report [22]. The excellent agreement between the experimental data and simulations suggests that the bilayer edges in our experiment (Fig. 2(a)) indeed have a reconstructed closed-loop structure and that the prominent pre-peak at 190.2 eV originates from dangling bonds of $sp^2$ hybridized boron atoms.

Having established that the dangling bond at boron atoms is responsible for the prominent pre-peak observed at the B K-edge ELNES at monolayer B-terminated zigzag edge, we further explore this spectroscopic signature at bilayer step edges. Figures 4(a) and 4(b) show the presence of step edges in a bilayer h-BN via sputtering off part of the bottom layer. The atomic configurations of the step edges can be deduced from the AA' stacking of the bilayer and the orientation of the exposed monolayer h-BN, as schematically shown in Fig. 4(c). Note that this model is used to highlight the overall edge structures as shown in Fig. 4(b), and some vacancies along the edges have been omitted for clarity. STEM-EELS line scans were acquired along the arrow direction at the top left corner of Fig. 4(c), crossing a B terminated zigzag step edge (see Fig. S5 in the ESM). Note that the ELNES obtained from the B-terminated step edge shows a similar pre-peak at 190.2 eV, but with weaker intensity than the $\pi^*$ peak. This feature is different from the observations in the monolayer case (Fig. 1(c)), but is also expected as the spectrum collected at the B-terminated step edge includes signals from the edge and the remaining top monolayer of h-BN. Therefore, the pre-peak at the step edge is inevitably weaker than that in monolayer B-terminated zigzag edges. These results further confirm that the pre-peak of the B K-edge arises from the unsaturated bonding of $sp^2$ B atoms at the edges.

## 4 Conclusions

In summary, the electronic states of B atoms at different types of edges in monolayer and bilayer h-BN are systematically investigated by a combination of aberration-corrected STEM imaging, atomically resolved STEM-EELS, and first-principles calculations. Spectroscopic signatures of edges with bonding unsaturated $sp^2$ B atoms, namely B-terminated zigzag monolayer edges and step edges, is unambiguously identified as a prominent pre-peak at 190.2 eV in the B K-edge ELNES. Spectroscopic fine structures from bilayer edges created *in-situ* via e-beam irradiation further confirm the previous report on closed-loop bilayer reconstructed edges. These spectroscopic signatures can serve as fingerprints to explore and identify new edge structures in h-BN. Our work also demonstrates that atomically resolved STEM-EELS combined with theoretical simulations provide a feasible means to probe the local electronic states in large bandgap 2D materials at the atomic scale.

## Acknowledgements

This research performed in the CAS Key Laboratory of Vacuum Sciences in University of Chinese Academy of Sciences is financially supported by the National Key R&D Program of China (No. 2018YFA0305800), the National Natural Science Foundation of China

(Nos. 51622211 and 51872284), the CAS Key Research Program of Frontier Sciences, the CAS Pioneer Hundred Talents Program, and Beijing Nova Program (No. Z181100006218023). The electron microscopy work was supported in part by Oak Ridge National Laboratory's Center for Nanophase Materials Sciences (CNMS), which is a DOE Office of Science User Facility. Work at Vanderbilt University was supported by U.S. Department of Energy grant DE-FG02-09ER46554 and by the McMinn Endowment.

**Electronic Supplementary Material**: Supplementary material (ADF image for quantification of monolayer and bilayer h-BN, additional STEM-EELS line scan data, and additional DFT calculation results) is available in the online version of this article at https://doi.org/10.1007/s12274-019-2417-5.

## References

[1] Jin, C. H.; Lin, F.; Suenaga, K.; Iijima, S. Fabrication of a freestanding boron nitride single layer and its defect assignments. *Phys. Rev. Lett.* **2009**, *102*, 195505.

[2] Alem, N.; Erni, R.; Kisielowski, C.; Rossell, M. D.; Gannett, W.; Zettl, A. Atomically thin hexagonal boron nitride probed by ultrahigh-resolution transmission electron microscopy. *Phys. Rev. B* **2009**, *80*, 155425.

[3] Gibb, A. L.; Alem, N.; Chen, J. H.; Erickson, K. J.; Ciston, J.; Gautam, A.; Linck, M.; Zettl, A. Atomic resolution imaging of grain boundary defects in monolayer chemical vapor deposition-grown hexagonal boron nitride. *J. Am. Chem. Soc.* **2013**, *135*, 6758–6761.

[4] Liu, Y. Y.; Zou, X. L.; Yakobson, B. I. Dislocations and grain boundaries in two-dimensional boron nitride. *ACS Nano* **2012**, *6*, 7053–7058.

[5] Tran, T. T.; Bray, K.; Ford, M. J.; Toth, M.; Aharonovich, I. Quantum emission from hexagonal boron nitride monolayers. *Nat. Nanotechnol.* **2016**, *11*, 37–41.

[6] Wang, Q. X.; Zhang, Q.; Zhao, X. X.; Luo, X.; Wong, C. P. Y.; Wang, J. Y.; Wan, D.; Venkatesan, T.; Pennycook, S. J.; Loh, K. P. et al. Photoluminescence upconversion by defects in hexagonal boron nitride. *Nano Lett.* **2018**, *18*, 6898–6905.

[7] Barone, V.; Peralta, J. E. Magnetic boron nitride nanoribbons with tunable electronic properties. *Nano Lett.* **2008**, *8*, 2210–2214.

[8] Li, Q. C.; Zou, X. L.; Liu, M. X.; Sun, J. Y.; Gao, Y. B.; Qi, Y.; Zhou, X. B.; Yakobson, B. I.; Zhang, Y. F.; Liu, Z. F. Grain boundary structures and electronic properties of hexagonal boron nitride on Cu(111). *Nano Lett.* **2015**, *15*, 5804–5810.

[9] Qi, Y.; Zhang, Z. P.; Deng, B.; Zhou, X. B.; Li, Q. C.; Hong, M.; Li, Y. C.; Liu, Z. F.; Zhang, Y. F. Irreparable defects produced by the patching of h-BN frontiers on strongly interacting Re(0001) and their electronic properties. *J. Am. Chem. Soc.* **2017**, *139*, 5849–5856.

[10] Grad, G. B.; Blaha, P.; Schwarz, K.; Auwärter, W.; Greber, T. Density functional theory investigation of the geometric and spintronic structure of h-BN/Ni(111) in view of photoemission and STM experiments. *Phys. Rev. B* **2003**, *68*, 085404.

[11] Suenaga, K.; Koshino, M. Atom-by-atom spectroscopy at graphene edge. *Nature* **2010**, *468*, 1088–1090.

[12] Suenaga, K.; Tencé, M.; Mory, C.; Colliex, C.; Kato, H.; Okazaki, T.; Shinohara, H.; Hirahara, K.; Bandow, S.; Iijima, S. Element-selective single atom imaging. *Science* **2000**, *290*, 2280–2282.

[13] Zhou, W.; Kapetanakis, M. D.; Prange, M. P.; Pantelides, S. T.; Pennycook, S. J.; Idrobo, J. C. Direct determination of the chemical bonding of individual impurities in graphene. *Phys. Rev. Lett.* **2012**, *109*, 206803.

[14] Suenaga, K.; Sato, Y.; Liu, Z.; Kataura, H.; Okazaki, T.; Kimoto, K.; Sawada, H.; Sasaki, T.; Omoto, K.; Tomita, T. et al. Visualizing and identifying single atoms using electron energy-loss spectroscopy with low accelerating voltage. *Nat. Chem.* **2009**, *1*, 415–418.

[15] Senga, R.; Komsa, H. P.; Liu, Z.; Hirose-Takai, K.; Krasheninnikov, A. V.; Suenaga, K. Atomic structure and dynamic behaviour of truly one-dimensional ionic chains inside carbon nanotubes. *Nat. Mater.* **2014**, *13*, 1050–1054.

[16] Tan, H. Y.; Turner, S.; Yücelen, E.; Verbeeck, J.; Van Tendeloo, G. 2D atomic mapping of oxidation states in transition metal oxides by scanning transmission electron microscopy and electron energy-loss spectroscopy. *Phys. Rev. Lett.* **2011**, *107*, 107602.

[17] Kimoto, K.; Asaka, T.; Nagai, T.; Saito, M.; Matsui, Y.; Ishizuka, K. Element-selective imaging of atomic columns in a crystal using STEM and EELS. *Nature* **2007**, *450*, 702–704.

[18] Ramasse, Q. M.; Seabourne, C. R.; Kepaptsoglou, D. M.; Zan, R.; Bangert, U.; Scott, A. J. Probing the bonding and electronic structure of single atom dopants in graphene with electron energy loss spectroscopy. *Nano Lett.* **2013**, *13*, 4989–4995.

[19] Lin, Y. C.; Teng, P. Y.; Chiu, P. W.; Suenaga, K. Exploring the single atom spin state by electron spectroscopy. *Phys. Rev. Lett.* **2015**, *115*, 206803.

[20] Warner, J. H.; Lin, Y. C.; He, K.; Koshino, M.; Suenaga, K. Atomic level spatial variations of energy states along graphene edges. *Nano Lett.* **2014**, *14*, 6155–6159.

[21] Suenaga, K.; Kobayashi, H.; Koshino, M. Core-level spectroscopy of point defects in single layer h-BN. *Phys. Rev. Lett.* **2012**, *108*, 075501.

[22] Alem, N.; Ramasse, Q. M.; Seabourne, C. R.; Yazyev, O. V.; Erickson, K.; Sarahan, M. C.; Kisielowski, C.; Scott, A. J.; Louie, S. G.; Zettl, A. Subangstrom edge relaxations probed by electron microscopy in hexagonal boron nitride. *Phys. Rev. Lett.* **2012**, *109*, 205502.

[23] Kim, K. K.; Hsu, A.; Jia, X. T.; Kim, S. M.; Shi, Y. M.; Hofmann, M.; Nezich, D.; Rodriguez-Nieva, J. F.; Dresselhaus, M.; Palacios, T. et al. Synthesis of monolayer hexagonal boron nitride on Cu foil using chemical vapor deposition. *Nano Lett.* **2012**, *12*, 161–166.

[24] Kresse, G.; Furthmüller, J. Efficient iterative schemes for *ab initio* total-energy calculations using a plane-wave basis set. *Phys. Rev. B* **1996**, *54*, 11169–11186.

[25] Blöchl, P. E. Projector augmented-wave method. *Phys. Rev. B* **1994**, *50*, 17953–17979.

[26] Buczko, R.; Duscher, G.; Pennycook, S. J.; Pantelides, S. T. Excitonic effects in core-excitation spectra of semiconductors. *Phys. Rev. Lett.* **2000**, *85*, 2168–2171.

[27] Duscher, G.; Buczko, R.; Pennycook, S. J.; Pantelides, S. T. Core-hole effects on energy-loss near-edge structure. *Ultramicroscopy* **2001**, *86*, 355–362.

[28] Dion, M.; Rydberg, H.; Schröder, E.; Langreth, D. C.; Lundqvist, B. I. Van der Waals density functional for general geometries. *Phys. Rev. Lett.* **2004**, *92*, 246401.